

Switching between Crystallization from the Glassy and the Undercooled Liquid Phase in Phase Change Material $\text{Ge}_2\text{Sb}_2\text{Te}_5$

Julian Pries, Shuai Wei, Matthias Wuttig,* and Pierre Lucas

Controlling crystallization kinetics is key to overcome the temperature–time dilemma in phase change materials employed for data storage. While the amorphous phase must be preserved for more than 10 years at slightly above room temperature to ensure data integrity, it has to crystallize on a timescale of several nanoseconds following a moderate temperature increase to near $2/3 T_m$ to compete with other memory devices such as dynamic random access memory (DRAM). Here, a calorimetric demonstration that this striking variation in kinetics involves crystallization occurring either from the glassy or from the undercooled liquid state is provided. Measurements of crystallization kinetics of $\text{Ge}_2\text{Sb}_2\text{Te}_5$ with heating rates spanning over six orders of magnitude reveal a fourfold decrease in Kissinger activation energy for crystallization upon the glass transition. This enables rapid crystallization above the glass transition temperature T_g . Moreover, highly unusual for glass-forming systems, crystallization at conventional heating rates is observed more than 50°C below T_g , where the atomic mobility should be vanishingly small.

Phase change materials (PCMs) such as $\text{Ge}_2\text{Sb}_2\text{Te}_5$ are ideal candidates for memory technologies due to i) their high contrast in conductivity and reflectivity between the crystalline and amorphous phase,^[1–3] ii) the rapid and reversible transformation between these two phases at elevated temperatures,^[4] and

iii) the stability of the amorphous phase near room temperature, which ensures data retention. The phase transformation is also accompanied by a change in bonding mechanism,^[5,6] in striking contrast to Zachariassen's conjecture that chemical bonds and, hence, the short-range order are identical in amorphous and crystalline solids.^[7] In PCMs, covalent bonding prevails in the amorphous phase, while a highly unconventional bonding mechanism called metavalent bonding (MVB)^[2,6,8] governs the atomic arrangement and properties of the crystalline state. Interestingly, PCM applications require that the kinetics of this unusual phase change must be controlled over a striking 16–17 orders of magnitude in time.^[1] In comparison, the most heavily characterized oxide glasses exhibit variations in crystallization time of less than ten


orders of magnitudes between the liquid and the glassy state.^[9] This immediately raises the question of what are the underlying factors governing this unusual crystallization kinetics.

Recently, emphasis has been devoted to an improved understanding of the undercooled liquid state, which revealed a transition in the temperature dependence of liquid dynamics.^[10,11] At the same time, a crucial property of glassy states, namely a calorimetric glass transition upon reheating at conventional rates ($\approx 0.1\text{--}100\text{ K min}^{-1}$), has not been detected yet;^[12] instead, the samples crystallize readily. Since the glass transition involves the arrest of atomic mobility at lower temperatures, it should drastically affect the crystallization kinetics of the system and its temperature dependence. The absence of a calorimetric glass transition in $\text{Ge}_2\text{Sb}_2\text{Te}_5$ has led to a wide spread reported values for the glass transition temperature T_g ranging from 100 to about 200°C .^[12–17] More importantly, this has caused contradicting interpretations regarding the phase from which the material crystallizes. On the one hand, calorimetric analyses of growth kinetics have been interpreted assuming that $\text{Ge}_2\text{Sb}_2\text{Te}_5$ crystallizes from the undercooled liquid (UCL).^[15,17,18] On the other hand, indirect measurements of crystallization speed based on PCM cell voltage have assumed crystallization taking place in the glassy state.^[14,19] Unambiguous experimental evidence for either possibility is currently missing since kinetic measurements alone do not permit clear characterization of a glass transition. We therefore

J. Pries, Dr. S. Wei, Prof. M. Wuttig
Institute of Physics IA
RWTH Aachen University
52074 Aachen, Germany
E-mail: wuttig@physik.rwth-aachen.de

Prof. M. Wuttig
Peter Grünberg Institute (PGI 10)
Forschungszentrum Jülich
52428 Jülich, Germany

Prof. P. Lucas
Department of Materials Science and Engineering
University of Arizona
Tucson, AZ 85712, USA

 The ORCID identification number(s) for the author(s) of this article can be found under <https://doi.org/10.1002/adma.201900784>.

© 2019 The Authors. Published by WILEY-VCH Verlag GmbH & Co. KGaA, Weinheim. This is an open access article under the terms of the Creative Commons Attribution-NonCommercial-NoDerivs License, which permits use and distribution in any medium, provided the original work is properly cited, the use is non-commercial and no modifications or adaptations are made.

DOI: 10.1002/adma.201900784

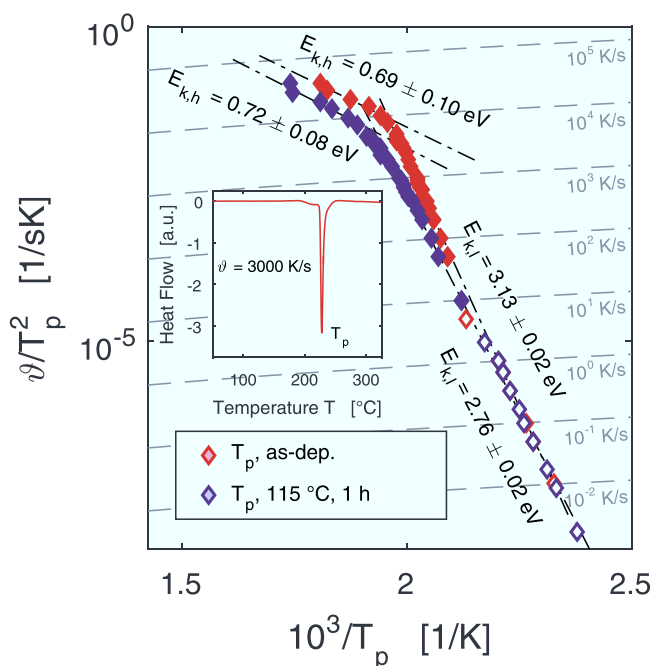


Figure 1. Kissinger plot for crystallization of $\text{Ge}_2\text{Sb}_2\text{Te}_5$. The peak temperature of crystallization T_p is measured as depicted in the inset for heating rates ranging from below 10^{-2} to $40\,000\text{ K s}^{-1}$. Each point is the average of at least ten measurements. The errors in E_k are the standard deviations from the fit procedure. Filled symbols are measured by ultrafast DSC and open symbols are measured by conventional DSC. Red symbols correspond to crystallization of the as-deposited state, while blue symbols represent crystallization of the $\text{Ge}_2\text{Sb}_2\text{Te}_5$ heat-treated for 1 h at 115 °C (preannealing). Values for the activation energy are obtained utilizing Equation (1). Two linear regimes are clearly distinguishable. The corresponding activation energy of crystallization E_k reveals a concomitant drop by a factor of four when exceeding $10\,000\text{ K s}^{-1}$.

use a combination of conventional and ultrafast differential scanning calorimetry (DSC and FDSC) to characterize the thermodynamic and kinetic signatures of the transition using a broad range of heating rates spanning over six orders of magnitude. The simultaneous analysis of the thermodynamic and kinetic response in combination with numerical simulations of crystallization permits us to unambiguously reveal the nature of the phase transformation.

In (F)DSC measurements of $\text{Ge}_2\text{Sb}_2\text{Te}_5$ at a constant heating rate, the thermodynamic response of crystallization is the dominant feature of the thermograms (see the inset of **Figure 1**). The corresponding crystallization peak temperature T_p depends upon the heating rate $\dot{\vartheta}$. The kinetic shift of T_p has long been the basis to characterize crystallization kinetics following the Kissinger method,^[20–23] where the Kissinger activation energy for crystallization E_k (i.e., the slope in a Kissinger plot) is obtained, according to

$$\ln\left(\frac{\dot{\vartheta}}{T_p^2} \cdot \text{sK}\right) = -\frac{E_k}{k_B T_p} + \ln\left(K_0 \frac{k_B}{E_k} \cdot \text{sK}\right) \quad (1)$$

where k_B is the Boltzmann constant and K_0 is the prefactor of the rate constant $K(T)$. The resulting Kissinger plot for as-deposited $\text{Ge}_2\text{Sb}_2\text{Te}_5$ shown in red in **Figure 1** covers an

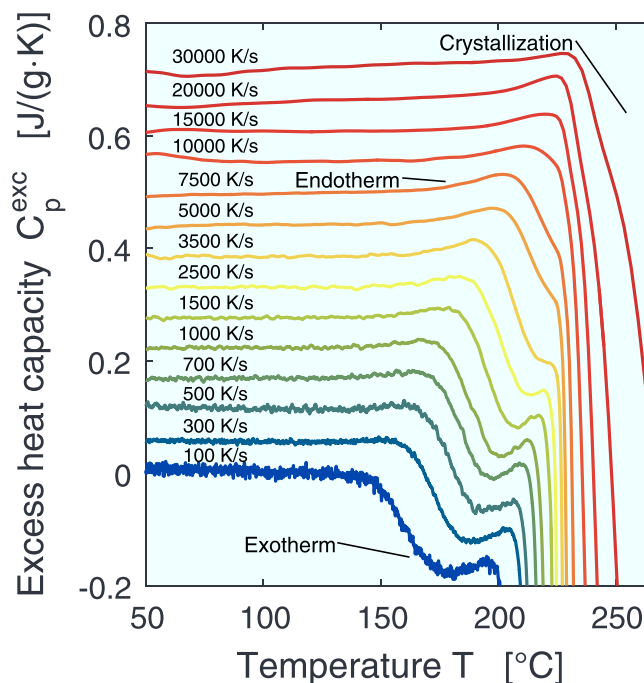


Figure 2. Selection of ultrafast DSC traces of as-deposited amorphous $\text{Ge}_2\text{Sb}_2\text{Te}_5$ as a function of temperature. Each trace is labeled with the corresponding heating rate. The traces obtained at lower rates exhibit a low temperature exotherm, which is a characteristic of the enthalpy release in quenched glasses while high heating rate traces exhibit an endotherm characteristic of complex relaxation processes near the glass transition. The exotherm due to crystallization is shown to shift to higher temperature with increasing heating rate. Each trace was subtracted by its subsequent rescan of the crystallized sample. Afterward, the crystallization exotherm was integrated and normalized to the heat of crystallization, which is found from DSC measurements to be 39.2 J g^{-1} (46.4 meV per atom), resulting in the given traces of excess heat capacity C_p^{exc} . The disappearance of the exothermic enthalpy relaxation in the FDSC traces coincides with the fourfold drop in the activation energy of crystallization E_k from 3.13 to 0.69 eV shown in **Figure 1**.

unprecedented six orders of magnitude at a total of 32 different heating rates, each repeated at least 10 times for good statistics. Because of the high data density in **Figure 1**, two linear regimes with distinct activation energies are clearly distinguished. The transition between the two regimes occurs near $10\,000\text{ K s}^{-1}$ and is associated with a drop in E_k by more than fourfold. A similar sharp change in crystallization kinetics has also been derived from cell voltage measurements.^[19] Such a drastic and sudden change in crystallization kinetics must have a profound microscopic origin. However, the kinetic measurements presented in **Figure 1** alone do not permit to identify the origin of the distinct kink between the two temperature dependencies of crystallization kinetics. Instead, it is necessary to gain insight by combining information on thermodynamics and kinetics supported by transmission electron microscopy (TEM) and numerical simulations, as discussed in the following.

Figure 2 shows the excess heat capacity C_p^{exc} of as-deposited $\text{Ge}_2\text{Sb}_2\text{Te}_5$ PCM films measured by FDSC over a wide range of heating rates $\dot{\vartheta}$. The thermal signals exhibit three notable thermodynamic features. First, the crystallization exotherm of the cubic phase is clearly apparent above 200 °C and is shown to

shift to higher temperatures with increasing ϑ . Only its onset is shown in Figure 2, as it overwhelms the signal (Figure 1 inset). Note that the onset of the cubic–trigonal phase transition is about 350 °C at a heating rate of 40 K min^{−1} (see Figure S16 in the Supporting Information), which is well above the peak temperature of the amorphous–cubic transition at all heating rates applied in this study (e.g., $T_p \approx 300$ °C for 40 000 K s^{−1}). Thus, the cubic phase is the relevant phase to the crystallization processes probed by the FDSC scans.

Second, a pronounced exotherm at low temperatures prior to crystallization is apparent up to 10 000 K s^{−1}. This is the characteristic of glasses obtained by quenching at a much faster cooling rate than the reheating rate. This exotherm is a signature of the high fictive temperature T_f of systems trapped far out of equilibrium,^[24–26] corresponding to high enthalpy glassy states with short structural relaxation times, thereby allowing significant enthalpy relaxation during the course of the slow reheating. As ϑ increases, the experimental timescale is reduced and, thus, enthalpy relaxation progressively shifts to higher temperature, until it eventually vanishes near 10 000 K s^{−1}. It is worth noting that the onset of crystallization overlaps with that exotherm and that both shift concomitantly with increasing ϑ .

The third feature of interest in Figure 2 is the endotherm prior to crystallization that develops by increasing ϑ above 700 K s^{−1}. This endotherm is a well-known effect called “shadow glass transition” which results from the broad distribution of relaxation times in fragile glasses^[24,25,27,28] and is commonly associated with density fluctuations.^[29] During fast cooling, slow relaxing domains get trapped in high T_f states while fast relaxing domains get trapped in low T_f states.^[29] Upon reheating, the fast domains can start regaining enthalpy while slow domains still need to release enthalpy. These opposite relaxation processes lead to the endotherm and subsequent exotherm apparent in Figures 2 and 3. The endotherm is exacerbated by higher nonexponentiality (higher fragility),

higher quenching rates, and preannealing.^[28] This effect should not be confused with the glass transition. In Figure 3a, their difference is demonstrated experimentally for the conventional glass-former GeSe, where, in contrast to Ge₂Sb₂Te₅, crystallization does not obscure the glass transition (see Figure 3a). The development of an endotherm onset far below the glass transition of 295 °C in GeSe is clearly observed after preannealing, which constitutes the shadow glass transition.^[25,30] Upon increasing preannealing, this transition merges with the actual glass transition as previously reported for oxide and metallic glasses.^[25,31] As shown in Figure 3b, a similar shadow glass transition introduced by annealing is also observed for Ge₂Sb₂Te₅, but is rapidly obscured by crystallization before the glass transition can be revealed. The developing endotherm after annealing was previously identified as the onset of the glass transition for several PCMs^[12] which leads to a significant underestimation of T_g as demonstrated in Figure 3. Thus, at slow heating rates, crystallization in Ge₂Sb₂Te₅ is initiated and proceeds below T_g , and hence within the glassy phase.

While crystallization obscures the glass transition of Ge₂Sb₂Te₅ at conventional heating rates, much higher rates can be reached by FDSC. Increasing the heating rate shifts crystallization to higher temperatures and could help to reveal the onset of the glass transition. The (F)DSC traces at heating rates <10 000 K s^{−1} in Figures 2,3 clearly indicate that the exothermic enthalpy relaxation process in Ge₂Sb₂Te₅ has not yet been completed at the time crystallization starts. Yet, a quenched system can only relax exothermically, if it is still far out of equilibrium and consequently still a glass. If it were already in the UCL, there would be no driving force for such an enthalpy relaxation, especially not at low ϑ where ergodicity would have been easily established. On the contrary, when the heating rate exceeds ≈ 10 000 K s^{−1}, the enthalpy relaxation exotherm vanishes completely (Figure 2, upper curves). Instead, FDSC traces indeed exhibit only a glass-transition-like endotherm prior to

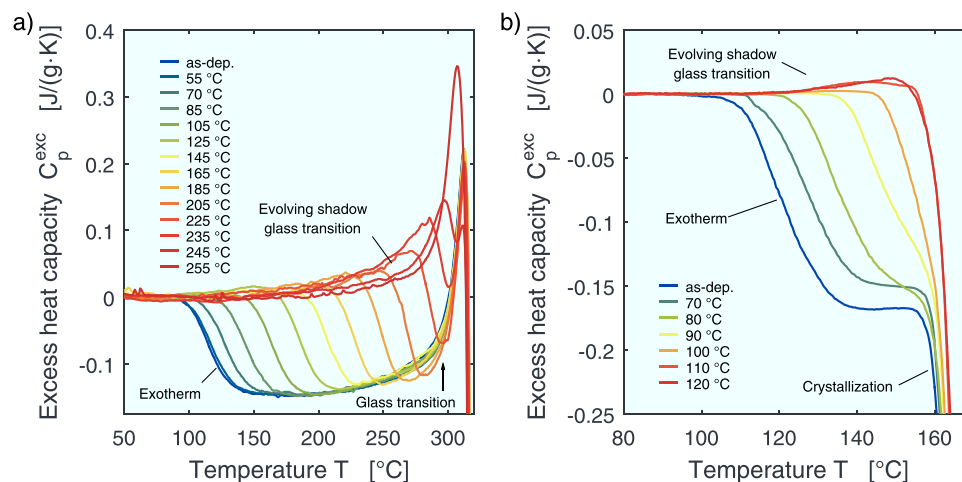


Figure 3. Shadow glass transition in annealed GeSe and Ge₂Sb₂Te₅ glasses. a,b) DSC curves of GeSe (a) and Ge₂Sb₂Te₅ (b) after preannealing. Each trace is baseline-corrected using the corresponding crystalline thermogram and therefore constitutes the excess heat capacity C_p^{exc} . All heating rates are 40 K min^{−1}. As-deposited films of both GeSe (a) and Ge₂Sb₂Te₅ (b) release an increasing amount of trapped enthalpy during annealing for 1 h at increasing temperatures which leads to a vanishing of the exotherm in the subsequent upscan shown in this figure. While the glass transition of GeSe (a) is clearly visible at 295 °C, it is obscured by the crystallization exotherm in Ge₂Sb₂Te₅ (b). Depending on annealing conditions, a shadow glass transition is introduced in both GeSe (a) and Ge₂Sb₂Te₅ (b) well below the actual temperature of the glass transition. The glass transition is visible only for GeSe (a), but is obscured by crystallization in Ge₂Sb₂Te₅ (b).

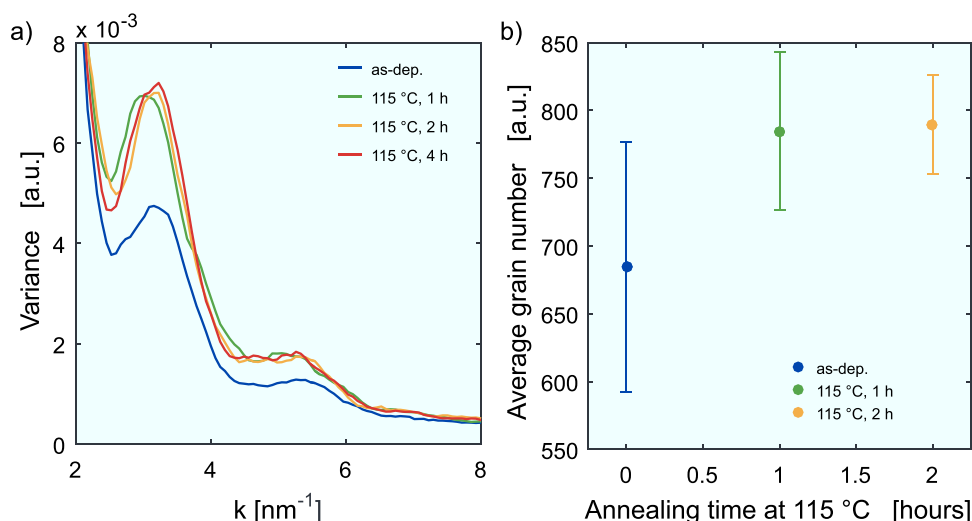


Figure 4. a) FEM variance of $\text{Ge}_2\text{Te}_2\text{Sb}_5$ as a function of scattering vector k and b) the average number of grains found from TEM for different preannealing states. a) The FEM variance curves are calculated from 1100 to 1400 diffraction patterns for each annealing state. The variance peak at about 3.2 nm^{-1} increases with preannealing time at 115°C . Most of the increase occurs in the first hour of annealing. An increase in variance indicates an increase in medium range order (MRO), which might be correlated with the population of subcritical nuclei and thus the probability for crystal nucleation. b) The average number of grains in $\text{Ge}_2\text{Sb}_2\text{Te}_5$ samples after preannealing at 115°C and subsequent isothermal heating at 150°C for 1 h for full crystallization are plotted versus the preannealing time. The analysis of TEM images and a graph of the average grain size are provided in the Supporting Information. As in the FEM measurements in (a), also here in (b), most of the change occurs during the first hour of preannealing at 115°C . b) The increase in average number of grains confirms the increase in population of subcritical nuclei by preannealing as the main source for (a) increased MRO measured by FEM.

crystallization. This provides a consistent interpretation of the combined kinetic and thermodynamic data of Figures 1–3. The data at $\vartheta < 10\,000 \text{ K s}^{-1}$ in Figure 1 corresponds to the (F)DSC traces exhibiting a noticeable relaxation exotherm, as seen in Figure 2. Hence, the kinetic and thermodynamic behavior is consistent with $\text{Ge}_2\text{Sb}_2\text{Te}_5$ crystallizing from a glassy phase at low heating rates ($<10\,000 \text{ K s}^{-1}$). The fact that the change in E_k occurs at about the same ϑ as the disappearance of the enthalpy relaxation exotherm supports this argument.

If instead amorphous $\text{Ge}_2\text{Sb}_2\text{Te}_5$ was crystallizing from the UCL, preannealing should lead to faster crystallization. Preannealing is commonly applied to study nucleation rates I as it permits to intentionally manipulate the population of subcritical nuclei and thus the probability to nucleate.^[21] If the subcritical nuclei population increases (so-called priming), I increases which results in a lower T_p , and vice versa, for a decrease in subcritical nuclei population (so-called fading).^[21,22] In $\text{Ge}_2\text{Sb}_2\text{Te}_5$, priming and fading are both possible.^[32,33] To clarify, we measure how preannealing at 115°C for 1 h affects the medium range order (MRO) and crystallization kinetics for as-deposited $\text{Ge}_2\text{Sb}_2\text{Te}_5$ samples by fluctuation electron microscopy (FEM) and TEM, respectively. This annealing temperature is chosen to ensure that the temperature is high enough for the largest possible enthalpy relaxation, and is low enough to avoid crystallization. In FEM, the variance in scattered intensity as a function of scattering vector k is calculated (see the Supporting Information). This variance is proportional to the amount of MRO.^[34] As shown in Figure 4a, the FEM variance peak height at $k \approx 3.2 \text{ nm}^{-1}$ increases with preannealing. Therefore, preannealing of $\text{Ge}_2\text{Sb}_2\text{Te}_5$ leads to an increase in MRO. Most of this increase appears to occur in the first hour of annealing, and saturates subsequently.

If this increase in MRO corresponds to an increase in population of subcritical nuclei as proposed for PCMs including $\text{Ge}_2\text{Sb}_2\text{Te}_5$,^[32] this should result in a higher probability for crystal nucleation and thus in more grains in the fully crystallized material. Fully crystallized thin films can be imaged via TEM. To find the average number of grains as a function of preannealing time, samples of 30 nm thick $\text{Ge}_2\text{Sb}_2\text{Te}_5$ were preannealed also at 115°C for 1 and 2 h and subsequently crystallized at 150°C . From an analysis of the TEM images, the average number of grains (Figure 4b) and their size were estimated (see Figure S12 in the Supporting Information). The increase in the average number of grains with increasing preannealing is clearly visible in Figure 4b. Like for the MRO, most of the increase in the number of grains occurs during the first hour of preannealing. The correlation between MRO and the number of grains supports the claim that the MRO measured by FEM corresponds to the population of subcritical nuclei. Both increase upon preannealing (priming) leading to a higher probability of crystal nucleation.

From the increased probability of crystal nucleation, we would expect lower T_p values and shorter crystallization times upon preannealing. However, in stark contrast to this expectation, crystallization is actually delayed to higher temperatures by preannealing (Figure 1, blue symbols). The effect of further preannealing treatments at constant temperature and constant heating rate crystallization is provided in Figures S7 and S9 (Supporting Information). This observation is incompatible with crystallization from the UCL. However, in a glass, preannealing below T_g leads to an increase in viscosity η due to the reduction in configurational entropy S_c described by the Adam–Gibbs relation^[35]

$$\eta = \eta_0 \exp\left(\frac{B}{TS_c}\right) \quad (2)$$

where η_0 and B are constants. The configurational entropy S_c is proportional to the excess entropy S_{exc} .^[36] The S_{exc} can be calculated from the difference in excess heat capacity^[11] ΔC_p^{exc} between the as-deposited and preannealed C_p^{exc} curve given in Figure 3b. Integrating $\Delta C_p^{\text{exc}}/T$ in between the onset temperatures of enthalpy relaxation and crystallization, 80 and 160 °C, respectively, yields a loss in excess entropy S_{exc} of more than 18 mJ g⁻¹ K⁻¹ (0.25 k_B atom⁻¹). This causes a significant increase in η of the annealed glass. Such an increase in η upon thermal treatment has been demonstrated experimentally in fast-quenched chalcogenide systems such as infrared fibers.^[37] Given that crystal growth velocity v and nucleation rate I are both inversely proportional to η ,^[14,17,38–40] an increase in crystallization time (Figure S7, Supporting Information) and in T_p then ensues (Figure 1; Figure S9, Supporting Information). This decrease in crystallization kinetics is more pronounced at higher heating rate which causes a larger difference in T_p (Figure 1), and thus, the apparent change in E_k from 3.13 to 2.76 eV for the as-deposited and the preannealed Ge₂Sb₂Te₅, respectively. This observation further supports the hypothesis of crystallization from the glassy phase at $\vartheta < 10\,000$ K s⁻¹.

Notably, E_k of as-deposited and preannealed Ge₂Sb₂Te₅ in the high ϑ regime is essentially the same within the error (0.69 ± 0.10 and 0.72 ± 0.08 eV, respectively) (Figure 1), suggesting thermal history-independent crystallization kinetics. This is consistent with crystallization from the UCL, and therefore, the kink observed at ≈10 000 K s⁻¹ must correspond to an emerging glass transition. To explain, why E_k drops upon the emerging glass transition and why an offset in T_p values persists for crystallization at heating rates above 10 000 K s⁻¹, numerically simulations of the crystallization process are required.

In order to verify that preannealing leaves E_k unaffected when crystallization occurs in UCL, a similar Kissinger analysis for GeSe was performed. Here, T_p was measured for as-deposited GeSe and compared to that of GeSe preannealed at 165 °C for 1 h. During the preannealing, an excess entropy of 37.1 mJ g⁻¹ K⁻¹ (0.338 k_B atom⁻¹) is released; therefore, the isoconfigurational η of the glassy phase is increased. GeSe behaves as a conventional glass crystallizing from the UCL after undergoing a glass transition even at low heating rates (Figure 3a). Since crystallization occurs from the UCL, thermal treatment below $T_g = 295$ °C should not affect the activation energy of crystallization E_k in GeSe, but may lead to a possible change in T_p due to a variation in subcritical nuclei population. As can be seen in Figure 5, no significant change in T_p is induced upon preannealing indicating only marginal changes in the subcritical nuclei population. Most importantly, E_k before and after preannealing is identical, and there is no discontinuity in E_k . Rather, a progressive curvature in the Kissinger plot is observed before and after preannealing. These observations are in line with expectations for systems crystallizing only from the (undercooled) liquid state.^[23,41] The distinct differences between GeSe (crystallizing from the UCL) observed in Figure 5 and Ge₂Sb₂Te₅ seen in Figure 1 then unambiguously

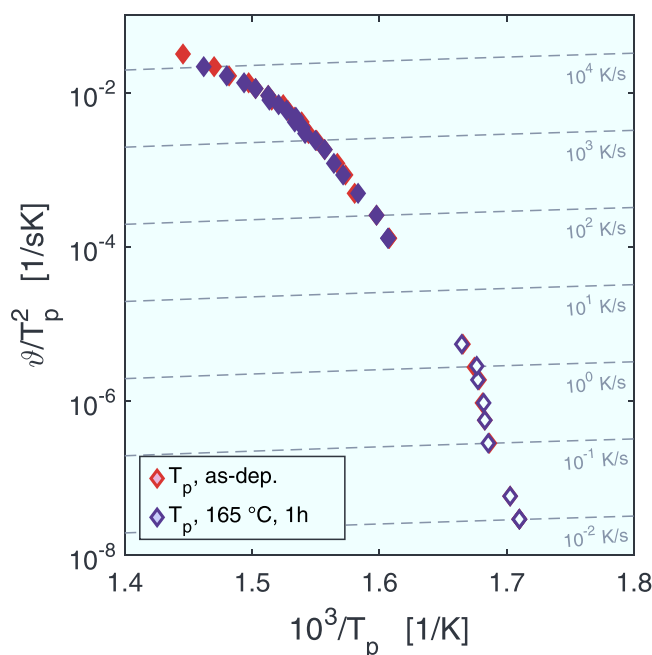


Figure 5. Kissinger plot for crystallization of GeSe. Red symbols correspond to crystallization of the as-deposited glass, while blue symbols correspond to crystallization of the glass heat-treated for 1 h at 165 °C. From conventional DSC measurements, the enthalpy of crystallization is found to be 43.5 J g⁻¹ (34.2 meV atom⁻¹). No abrupt change in activation energy of crystallization E_k but rather a continuous curvature is present in both as-deposited and preannealed GeSe. Moreover, there is no significant difference in crystallization kinetics between both states.

confirm that Ge₂Sb₂Te₅ crystallizes from a glassy phase at rates below ≈10 000 K s⁻¹, where E_k differs from as-deposited and preannealed Ge₂Sb₂Te₅.

Overall, the results of Figures 1–5 show that the endotherm observed for Ge₂Sb₂Te₅ at heating rates higher than 10 000 K s⁻¹ corresponds to the emerging glass transition. However, it is measured at extremely high rates and likely only constitutes the onset of the transition. Therefore, we still lack a reliable estimate for the standard T_g defined at a rate of 20 K min⁻¹. In order to derive a more precise value, we use the plot of Velikov et al. to estimate T_g from the enthalpy relaxation dynamics of hyperquenched glasses.^[42] Figure 6 compares the excess heat capacity of a series of hyperquenched bulk glass formers with well-established T_g values. The temperature axis is scaled by T_g to enable comparison over a wide variety of glass formers including oxides, metallic, and molecular glasses spanning over a wide range of T_g and the full range of fragility. It is found that the enthalpy recovery exotherm of all glasses reaches a maximum near $T/T_g = 0.85$ –0.95. This provides means of estimating the T_g of Ge₂Sb₂Te₅ using its enthalpy recovery exotherm. Choosing a value of T/T_g for the exotherm maximum comparable to that of orthoterphenyl because of similar reported fragility values^[17,42] yields $T_g = 200 \pm 10$ °C. This T_g value supports the conclusion that Ge₂Sb₂Te₅ crystallizes from the glassy state when reheated slowly (<10 000 K s⁻¹). Indeed, its onset of crystallization is ≈150 °C at 20 K min⁻¹, being roughly 50 °C below the standard glass transition temperature T_g at 20 K min⁻¹. As shown in Figure 6, a value of $T_g = 110$ °C far below the

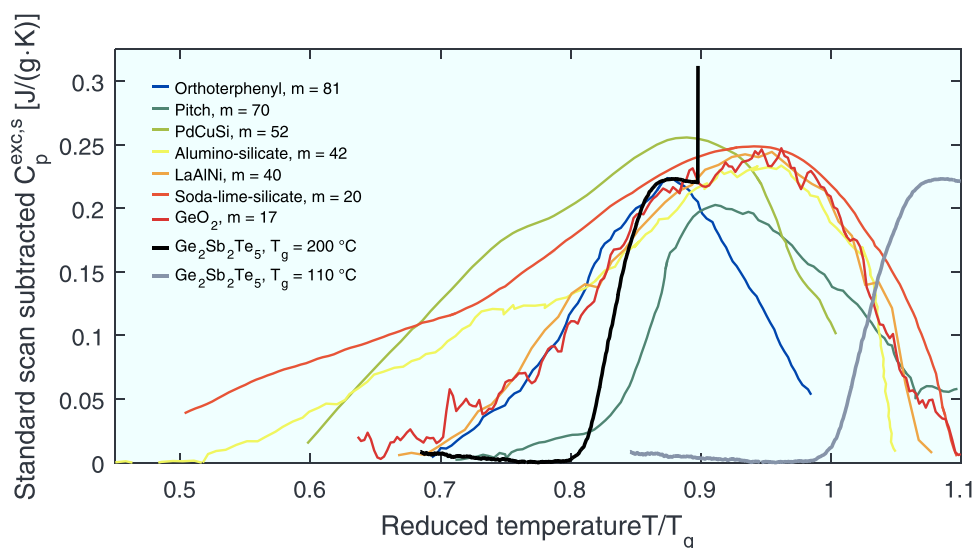


Figure 6. Estimation of the standard T_g value of $\text{Ge}_2\text{Sb}_2\text{Te}_5$ using the hyperquench method. The enthalpy recovery exotherm is shown for a wide variety of hyperquenched glasses including oxide, metallic, and molecular glasses over a broad range of T_g (246–944 K) and a broad range of fragility ($m = 20$ –81). Orthoterphenyl,^[42] pitch,^[46] $\text{Pd}_{77.5}\text{Cu}_6\text{Si}_{16.5}$,^[47] $\text{La}_{55}\text{Al}_{25}\text{Ni}_{20}$,^[26] basaltic fiber (SiO_2 : 49.3, Al_2O_3 : 1.8; FeO : 11.7; CaO : 10.4; MgO : 3.9; Na_2O : 3.9; K_2O : 0.7),^[48] soda lime–silicate (SiO_2 : 70.5; Na_2O : 8.7; K_2O : 7.7; CaO : 11.6; Sb_2O_3 : 1.1; SO_3 : 0.2),^[49] and GeO_2 .^[50] All glasses show a maximum of enthalpy release near $T/T_g \approx 0.9$. If the glass transition of $\text{Ge}_2\text{Sb}_2\text{Te}_5$ is set to be $T_g = 110$ °C, the maximum of the enthalpy release would be above T_g (gray line). Setting a value of T/T_g for the enthalpy release maximum comparable to that of orthoterphenyl due to similar reported fragility values yields $T_g = 200 \pm 10$ °C (black curve).

crystallization onset as previously suggested^[15,17] would signify that the system is still slowly relaxing even through it is already in the ergodic UCL state well above T_g . Such a low value of T_g is therefore not compatible with the general relaxation kinetics of glasses. Utilizing the T_g value of 200 °C, as derived here, and viscosity data of liquid $\text{Ge}_2\text{Sb}_2\text{Te}_5$,^[43] we find $m = 98$ by Mauro–Yue–Ellison–Gupta–Allan (MYEGA) function fitting^[44] (see Figure S5 in the Supporting Information). This conclusion is consistent with the fragility value of $m = 90$ reported earlier.^[17]

As shown in Figure 2, the enthalpy relaxation exotherm has completely vanished at $\vartheta \approx 20\,000\text{ K s}^{-1}$. Hence, this ϑ value should be close to an effective cooling rate attributed to the sputter deposition process. If the cooling rate is equal to the heating rate, the apparent glass transition temperature T_g is equal to the fictive temperature T_f . For a consistency check, a value of T_g for a rate of $20\,000\text{ K s}^{-1}$ can be approximated using the Moynihan method for the rate dependence of T_f ^[45] making use of the values determined for m and T_g (see the Supporting Information). This approximation yields 224 °C consistent with the endotherm onset in the FDSC scan of $20\,000\text{ K s}^{-1}$ observed in Figure 2. Therefore, the fourfold drop in activation energy E_k corresponds to the emerging glass transition at $\vartheta > 10\,000\text{ K s}^{-1}$.

In the classical picture, near T_g glasses usually have a lower activation energy of viscous flow than the UCL, because the atomic configuration is frozen-in by vitrification. Thus, according to the Adam–Gibbs equation (Equation (2)), an approximately constant configurational entropy S_c only leads to an Arrhenius behavior of viscosity of constant activation energy, while in the UCL, the activation energy decreases with increasing temperature. Since the crystal growth velocity v and nucleation rate I are inversely proportional to the viscosity η , the activation energy E_k would be

lower in glasses than in the UCL. The observed fourfold drop in activation energy E_k upon emerging glass transition at a heating rate of $\approx 10\,000\text{ K s}^{-1}$ appears to be inconsistent with this classical picture. However, this is a consequence of probing a high-fragility system with an unconventionally high heating rate. The rate is high enough to probe the high-temperature regime where the activation energy of viscosity becomes much lower (see Figure S3 in the Supporting Information), compared to that of the glass sampled at a lower rate. To gain a deeper insight, we perform numerical simulations of the crystallization behavior as an attempt to reproduce the experimental observations from (F)DSC. The simulation is based on evaluating the Johnson–Mehl–Avrami–Kolmogorov (JMAK) model for crystallization at constant heating rate similar to refs. ^[18,23]. In the JMAK model, the variation of the crystallized volume fraction is controlled by the rate constant K that is composed of crystal growth velocity v and nucleation rate I . The crystallized volume fraction should be proportional to the enthalpy being released during crystallization,^[51] which can be used to simulate the heat capacity peak temperature of crystallization (T_p). Details of these simulations are presented in the Supporting Information.

First, crystallization is simulated for the glassy phase to validate the simulation method. Since the experimental T_p values of the glassy phase (below $10\,000\text{ K s}^{-1}$) follow an Arrhenius-like ϑ dependence, the temperature dependence of the rate constant $K(T)$ also has to be Arrhenius-like,^[52] i.e.,

$$K(T) = K_0 \exp(-E_k/k_B T) \quad (3)$$

Using the prefactor K_0 and the activation energy E_k found from fitting Equation (1) (Figure 1), crystallization is simulated (see the Supporting Information). The resulting T_p values are

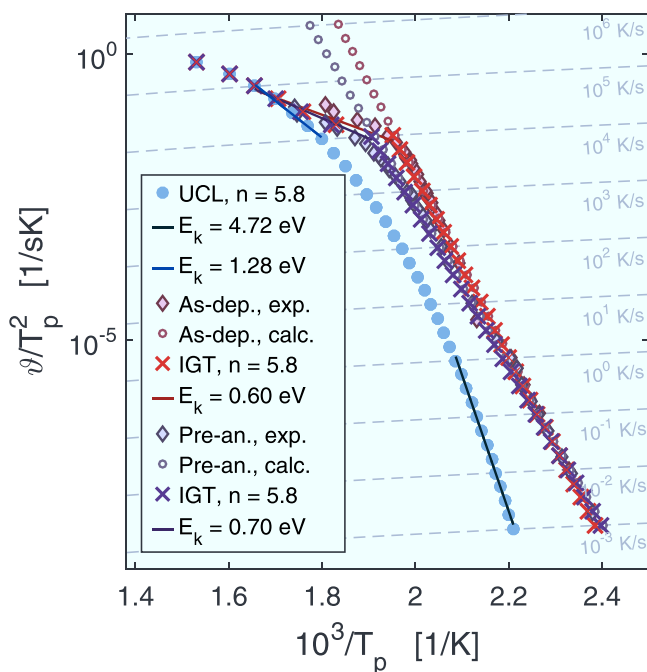


Figure 7. Kissinger plot of experimental and numerically simulated crystallization peak temperature T_p . Open circles represent T_p values numerically simulated based on the parameters found from fitting Equation (1) to experimental T_p data below $10\,000\text{ K s}^{-1}$ (Figure 1), which show excellent agreement. For calculating the T_p values for the UCL (blue full circles), the MYEGA model for viscosity η , $T_g = 200\text{ °C}$, $m = 98$, and the Avrami exponent $n = 5.8$ are used (see the Supporting Information). For rates in between 10^{-3} and 10^0 K s^{-1} , the Kissinger activation energy E_k for the UCL is 4.72 eV, which is higher than the E_k values found for experimental data of the glassy phase (3.13 and 2.76 eV, Figure 1), confirming the classical picture. Below $10\,000\text{ K s}^{-1}$, the UCL T_p values do not align with experimental values and show a curvature that is not observed in experiments (diamonds in background), since here crystallization occurs from a glassy phase. However, at higher heating rates the T_p values of the UCL do also not align with the experimental data. Only when a glass transition is introduced in the simulations at $T = T_p$ ($10\,000\text{ K s}^{-1}$) by instantaneously changing the temperature dependence of crystallization from glass like to UCL like in the IGT model developed, the simulated T_p values (crosses) resemble the experimental T_p data and the observed drop in activation energy E_k is reproduced.

shown in **Figure 7** (open circles) alongside experimental data (full diamonds, same data as in Figure 1), which show excellent agreement below $10\,000\text{ K s}^{-1}$. This confirms the validity of the simulation method.

Then, crystallization is simulated for the UCL, based on the T_g and fragility values found in this work, the MYEGA model for viscosity η , and an Avrami exponent $n = 5.8$ (see the Supporting Information). The calculated T_p values for the UCL (full circles) show a continuous change in slope, as reported in ref. [23], indicating a decrease in E_k as ϑ as increases. Between 10^{-3} and 10^0 K s^{-1} , E_k in the UCL on average is 4.72 eV. The experimental E_k values of glassy states (i.e., $E_k = 3.13\text{ eV}$ (as-deposited) and 2.76 eV (preannealed)) are significantly smaller than that for the UCL in the corresponding ϑ regime. Hence, for crystallization at heating rates accessible to conventional DSC up to $\approx 10^0\text{ K s}^{-1}$, $E_k(\text{UCL}) > E_k(\text{glass})$, as expected from the classical picture. Below $10\,000\text{ K s}^{-1}$, the curved heating rate dependence of

simulated T_p values for UCL does not agree with the Arrhenius-like experimental data, indicating that the measured data do not correspond to the UCL. With increasing ϑ , in the range between 10^4 and 10^5 K s^{-1} , the E_k value for the UCL decreases continuously to 1.28 eV. As the heating rate ϑ is increased further, the simulated activation energy approaches the experimental values of 0.67 eV (as-deposited) and 0.71 eV (preannealed). Nevertheless, the experimental and simulated T_p values for the UCL do not equalize. Below $10\,000\text{ K s}^{-1}$ this is expected because $\text{Ge}_2\text{Sb}_2\text{Te}_5$ crystallizes from a glassy phase and not from the UCL. Above $10\,000\text{ K s}^{-1}$, glass transition and crystallization interfere, which is accounted for in the simulation model developed below.

To account for an emerging glass transition as ϑ exceeds $10\,000\text{ K s}^{-1}$, the simulations are modified. The temperature dependence of nucleation rate $I(T)$ and crystal growth velocity $v(T)$ is instantaneously switched from glass-like to UCL-like at the experimental T_p value at $10\,000\text{ K s}^{-1}$ (i.e., $T_p = 242\text{ °C}$ (as-deposited) and 261 °C (preannealed)). This instantaneous glass transition (IGT) model surely is a simplification since the glass transition usually spans over a temperature interval of certain width. However, the T_p values simulated under this assumption (crosses in Figure 7) and the experimental T_p agree fairly well. Moreover, the activation energy E_k values of the modeled T_p values between 10^4 and 10^5 K s^{-1} are now 0.60 eV (as-deposited) and 0.70 eV (preannealed). The simulated E_k values for the IGT model are now almost equal to the experimental values of 0.69 eV (as-deposited) and 0.72 eV (preannealed). Therefore, the kink in experimental T_p values while exceeding $10\,000\text{ K s}^{-1}$ is a manifestation of the interference of glass transition and crystallization. Hence, despite its simplifications, the IGT model for the transition from glass-like to UCL-like temperature dependence of crystallization permits us to reproduce the main experimental findings quantitatively.

Accordingly, the offset in experimental T_p data of as-deposited and preannealed $\text{Ge}_2\text{Sb}_2\text{Te}_5$ above $10\,000\text{ K s}^{-1}$ stems only from the modification of the glassy phase introduced by preannealing. When exceeding $100\,000\text{ K s}^{-1}$, the T_p values of the IGT (crosses) overlap with those of the UCL (full circles) (Figure 7), indicating crystallization being fully dominated by the temperature dependence of the UCL. Also, in this regime, the difference in T_p of as-deposited and preannealed samples vanishes as expected. So, below $10\,000\text{ K s}^{-1}$, $\text{Ge}_2\text{Sb}_2\text{Te}_5$ crystallizes from the glassy phase alone whereas above that rate the drastic decrease in activation energy E_k is caused by the emerging glass transition during ongoing crystallization.

Crystallization kinetics of $\text{Ge}_2\text{Sb}_2\text{Te}_5$ have been analyzed for heating rates ϑ spanning more than six orders of magnitude. The corresponding data reveal a fourfold drop in activation energy E_k . We attribute the drop in E_k to the transition from crystallization of a glassy phase below $10\,000\text{ K s}^{-1}$ to crystallization of the UCL state above it. The thermodynamic analyses of (F)DSC traces show the presence of enthalpy relaxation in $\text{Ge}_2\text{Sb}_2\text{Te}_5$ up to $10\,000\text{ K s}^{-1}$, which is a signature of a glassy phase. The vanishing enthalpy relaxation upon exceeding $10\,000\text{ K s}^{-1}$ coincides with the fourfold drop in E_k . This drop is reproduced when the crystallization process is simulated numerically, assuming a glass transition at $10\,000\text{ K s}^{-1}$. Thus, the fourfold drop in E_k is caused by the concurrence of crystallization and the glass transition. We note that the highest

heating rate of $40\,000\text{ K s}^{-1}$ accessible to the FDSC in this study is still a few orders of magnitude lower than that for crystallization in PCM device operations (up to $\approx 10^{10}\text{ K s}^{-1}$). Probing crystallization from UCL at even faster heating rates requires ultrafast techniques such as pump–probe X-ray, which may provide further insight into the fast switching behavior in PCM devices.

Furthermore, FEM and TEM measurements demonstrate an increased probability of crystal nucleation upon preannealing. For crystallization from a UCL, this would lead to a lower T_p . Instead, an increased T_p is observed in preannealed $\text{Ge}_2\text{Sb}_2\text{Te}_5$ demonstrating decreased crystallization speed. This observation can only be explained by crystallization from a glassy phase, where preannealing introduces aging and a higher viscosity of the glass, lowering atomic mobility. We emphasize that the glass transition is rate dependent. An estimation of T_g for a conventional rate of 20 K min^{-1} is about $200\text{ }^\circ\text{C}$. Combining the findings of kinetics, thermodynamics, microscopy, and numerical simulations, we conclude that $\text{Ge}_2\text{Sb}_2\text{Te}_5$ crystallizes from the glassy phase below $10\,000\text{ K s}^{-1}$, in contrast to previous claims.^[13,15,17,18,23,40]

The glass transition temperature of $200\text{ }^\circ\text{C}$ (at 20 K min^{-1}) is about $175\text{ }^\circ\text{C}$ above room temperature, which ensures the stability of the amorphous phase. Yet, T_g is low enough to easily enter the rapid crystallization regime of the UCL. Thus, in $\text{Ge}_2\text{Sb}_2\text{Te}_5$, T_g constitutes a key quantity to overcome the temperature–time dilemma. The fourfold drop in activation energy E_k associated with a heating rate of $\approx 10\,000\text{ K s}^{-1}$ permits us to identify the heating rate required to achieve ultrafast switching and allows for an optimization of the electrical pulse energy required to reset the memory element.

Crystallization is observed as low as $50\text{ }^\circ\text{C}$ below T_g at the heating rate of 20 K min^{-1} , where it intuitively should be inhibited by vanishing atomic mobility, exposing the strong tendency of PCMs to crystallize. Structural rearrangements like crystallization at these temperatures might relate to β -relaxation, which remains fast upon cooling below T_g .^[25,53]

Interestingly, $\text{Ge}_2\text{Sb}_2\text{Te}_5$ and glassy water both exhibit no clear calorimetric glass transition, since it is obscured by crystallization. Therefore, numerous values for T_g were proposed, ranging from 100 to $200\text{ }^\circ\text{C}$ and from 120 to 170 K ^[42] for $\text{Ge}_2\text{Sb}_2\text{Te}_5$ and water, respectively. Given the phenomenological analogy in the DSC scans between hyperquenched water and as-deposited $\text{Ge}_2\text{Sb}_2\text{Te}_5$, the finding of crystallization below T_g for $\text{Ge}_2\text{Sb}_2\text{Te}_5$ suggests that water may also crystallize below its T_g .

PCMs like $\text{Ge}_2\text{Sb}_2\text{Te}_5$, GeTe , and (Ag,In) -doped Sb_2Te_3 (AIST) generally show high fragilities and bad glass-forming abilities,^[38,54] while related chalcogenides like GeSe are non-PCMs that exhibit better glass-forming abilities with lower fragilities and the presence of a calorimetric glass transition.^[11] The question arises what is the origin of such distinctive differences between PCMs and non-PCMs, since GeTe and GeSe are isoelectronic and should hence have similar bonding mechanisms. Yet, it has recently been shown that contrary to this expectation, the bonding and properties of crystalline GeTe and GeSe differ significantly. As mentioned above, crystalline PCMs like GeTe or $\text{Ge}_2\text{Sb}_2\text{Te}_5$ possess a special bonding mechanism, namely, MVB, which is absent in the non-PCMs like GeSe .^[5,6] MVB is characterized by the competition between electron localization,

which characterizes covalent bonding, and delocalization, the hallmark of metallic bonding.^[6] Hence, for crystalline PCMs, a number of different possible atomic arrangements exist, which are quite similar in energy, but rather different in atomic arrangement and physical properties.^[5,55] This might manifest in amorphous PCMs as a rugged energy landscape, which has been related to liquid fragilities. This suggests that the high fragility, the distinct crystallization behavior, as well as the poor glass-forming ability in amorphous PCMs may be interwoven with the chemical bonding in their crystalline phases.

Experimental Section

In this work, amorphous $\text{Ge}_2\text{Sb}_2\text{Te}_5$ and GeSe samples were prepared via magnetron sputter deposition from stoichiometric targets utilizing a base pressure of $3 \times 10^{-6}\text{ mbar}$ and an argon gas flow of 20 sccm . The sputter deposition time was adjusted to yield a final thickness of about $3\text{ }\mu\text{m}$ for (F)DSC samples. The deposited materials were peeled from the substrates afterward. Conventional DSC was performed on a PerkinElmer Diamond DSC and ultrafast calorimetry on a Mettler–Toledo Flash DSC 1 (FDSC) utilizing heating rates $\dot{\theta}$ ranging from 0.008 to 5 K s^{-1} and from 10 to $40\,000\text{ K s}^{-1}$, respectively. The upper temperature limit of the FDSC was $450\text{ }^\circ\text{C}$. All (F)DSC data were corrected by the melting onset temperature of indium at the corresponding heating rate as described in the Supporting Information and shown in Figures S1 and S2 (Supporting Information). In this case and as already reported for $\text{Ge}_2\text{Sb}_2\text{Te}_5$, the Biot number was less than 0.1 ,^[15,17] indicating that thermal lag during FDSC measurements was negligible (see the Supporting Information). Utilizing a thermal conductivity for GeSe of about $1.2\text{ W m}^{-1}\text{ K}^{-1}$,^[56] a Biot number of 0.03 was found, which was also less than 0.1 and thus, thermal lag in GeSe can be neglected as well (see the Supporting Information).

Grain size measurements were performed on an FEI Tecnai F20 transmission electron microscope. The $\text{Ge}_2\text{Sb}_2\text{Te}_5$ layer of 30 nm is situated in between of two layers of amorphous capping material. All three layers were deposited by sputter deposition as described above on a substrate featuring a 50 nm thick Si_3N_4 electron transparent membrane. The as-deposited and preannealed samples (1 and 2 h at $115\text{ }^\circ\text{C}$) were brought to $150\text{ }^\circ\text{C}$ for 1 h to allow for full crystallization.

For FEM, 40 nm of $\text{Ge}_2\text{Sb}_2\text{Te}_5$ was directly sputtered onto an $\approx 8\text{ nm}$ thick amorphous carbon film which was supported by a copper grid. Four samples were measured in the as-deposited state, and in preannealed states ($115\text{ }^\circ\text{C}$ for 1 , 2 , and 4 h). FEM measurements were conducted on an FEI Titan G2 80–300 STEM. For each sample, 1100 – 1400 diffraction patterns were taken and utilized for calculating the variance in scattered intensity as a function of scattering vector k (see the Supporting Information for details).

The thermal treatment on the TEM samples for measuring the grain size and the FEM variance were performed under an argon atmosphere in the DSC.

Supporting Information

Supporting Information is available from the Wiley Online Library or from the author.

Acknowledgements

The authors acknowledge funding from the Deutsche Forschungsgemeinschaft (DFG) within the collaborative research center Nanoswitches (SFB 917). S.W. acknowledges the financial support from the A.v. Humboldt foundation and the RWTH Start-Up fund. J.P. thanks

Manuel Bornhöft at Gemeinschaftslabor für Elektronenmikroskopie (GfE), RWTH Aachen, for the introduction in FEM operation and Nelly Wirch (GfE) the support during FEM measurements. The authors are grateful to Stephan Hermes for engineering the sputter deposition TEM sample holder and to Christoph Persch and Martin Salinga for helpful discussions. P.L. acknowledges funding from the National Science Foundation (NSF) under Grant Nos. 1832817 and 1640860.

Conflict of Interest

The authors declare no conflict of interest.

Keywords

crystallization kinetics, glass transition temperature, phase change materials, structural relaxation, ultrafast differential scanning calorimetry (FDSC)

Received: January 31, 2019

Revised: July 12, 2019

Published online: August 6, 2019

- [1] M. Wuttig, N. Yamada, *Nat. Mater.* **2007**, 6, 824.
- [2] K. Shportko, S. Kremers, M. Woda, D. Lencer, J. Robertson, M. Wuttig, *Nat. Mater.* **2008**, 7, 653.
- [3] a) J. Y. Raty, W. Zhang, J. Luckas, C. Chen, R. Mazzarello, C. Bichara, M. Wuttig, *Nat. Commun.* **2015**, 6, 7467; b) S. Raoux, W. Welnic, D. Ielmini, *Chem. Rev.* **2010**, 110, 240.
- [4] a) S. R. Ovshinsky, *Phys. Rev. Lett.* **1968**, 21, 1450; b) J. Feinleib, S. R. Ovshinsky, *J. Non-Cryst. Solids* **1970**, 4, 564.
- [5] J. Y. Raty, M. Schumacher, P. Golub, V. L. Deringer, C. Gatti, M. Wuttig, *Adv. Mater.* **2019**, 31, 1806280.
- [6] M. Wuttig, V. L. Deringer, X. Gonze, C. Bichara, J. Y. Raty, *Adv. Mater.* **2018**, 30, 1803777.
- [7] W. H. Zachariasen, *J. Am. Chem. Soc.* **1932**, 54, 3841.
- [8] a) D. Lencer, M. Salinga, B. Grabowski, T. Hickel, J. Neugebauer, M. Wuttig, *Nat. Mater.* **2008**, 7, 972; b) M. Küpers, P. M. Konze, S. Maintz, S. Steinberg, A. M. Mio, O. Cojocaru-Mirédin, M. Zhu, M. Müller, M. Luysberg, J. Mayer, M. Wuttig, R. Dronskowski, *Angew. Chem., Int. Ed.* **2017**, 56, 10204.
- [9] B. P. Rodrigues, E. D. Zanotto, *J. Non-Cryst. Solids* **2012**, 358, 2626.
- [10] a) J. Orava, D. W. Hewak, A. L. Greer, *Adv. Funct. Mater.* **2015**, 25, 4851; b) S. Wei, G. J. Coleman, P. Lucas, C. Angell, *Phys. Rev. Appl.* **2017**, 7, 034035.
- [11] a) S. Wei, P. Lucas, C. A. Angell, *J. Appl. Phys.* **2015**, 118, 034903; b) S. Wei, Z. Evenson, M. Stolpe, P. Lucas, C. A. Angell, *Sci. Adv.* **2018**, 4, eaat8632.
- [12] J. A. Kalb, M. Wuttig, F. Spaepen, *J. Mater. Res.* **2007**, 22, 748.
- [13] J.-Y. Cho, D. Kim, Y.-J. Park, T.-Y. Yang, Y.-Y. Lee, Y.-C. Joo, *Acta Mater.* **2015**, 94, 143.
- [14] A. Sebastian, M. Le Gallo, D. Krebs, *Nat. Commun.* **2014**, 5, 4314.
- [15] B. Chen, G. H. ten Brink, G. Palasantzas, B. J. Kooi, *J. Phys. Chem. C* **2017**, 121, 8569.
- [16] a) M. H. R. Lankhorst, *J. Non-Cryst. Solids* **2002**, 297, 210; b) E. Morales-Sánchez, E. F. Prokhorov, A. Mendoza-Galván, J. González-Hernández, *J. Appl. Phys.* **2002**, 91, 697.
- [17] J. Orava, A. L. Greer, B. Gholipour, D. W. Hewak, C. E. Smith, *Nat. Mater.* **2012**, 11, 279.
- [18] J. Orava, A. L. Greer, B. Gholipour, D. W. Hewak, C. E. Smith, *Appl. Phys. Lett.* **2012**, 101, 091906.
- [19] R. Jayasingh, S. W. Fong, J. Lee, Z. Li, K.-W. Chang, D. Mantegazza, M. Asheghi, K. E. Goodson, H. S. P. Wong, *Nano Lett.* **2014**, 14, 3419.
- [20] D. W. Henderson, *J. Non-Cryst. Solids* **1979**, 30, 301.
- [21] C. S. Ray, D. E. Day, *J. Am. Ceram. Soc.* **1990**, 73, 439.
- [22] K. F. Kelton, *J. Am. Ceram. Soc.* **1992**, 75, 2449.
- [23] J. Orava, A. L. Greer, *Thermochim. Acta* **2015**, 603, 63.
- [24] Y. Yue, C. A. Angell, *Nature* **2004**, 427, 717.
- [25] L. Hu, Y. Yue, *J. Phys. Chem. C* **2009**, 113, 15001.
- [26] L. Hu, C. Zhang, Y. Yue, *Appl. Phys. Lett.* **2010**, 96, 221908/1.
- [27] I. M. Hodge, A. R. Berens, *Macromolecules* **1981**, 14, 1598.
- [28] I. M. Hodge, A. R. Berens, *Macromolecules* **1982**, 15, 762.
- [29] a) M. D. Ediger, *Annu. Rev. Phys. Chem.* **2000**, 51, 99; b) O. Gulbitten, J. C. Mauro, P. Lucas, *J. Chem. Phys.* **2013**, 138, 244504.
- [30] C. A. Angell, Y. Yuanzheng, W. Li-Min, R. D. C. John, B. Steve, M. Stefano, *J. Phys.: Condens. Matter* **2003**, 15, S1051.
- [31] a) L. Hornboll, T. Knusen, Y. Yue, X. Guo, *Chem. Phys. Lett.* **2010**, 494, 37; b) L. Hu, C. Zhou, C. Zhang, Y. Yue, *J. Chem. Phys.* **2013**, 138, 174508.
- [32] B.-S. Lee, R. M. Shelby, S. Raoux, C. T. Retter, G. W. Burr, S. N. Bogle, K. Darmawikarta, S. G. Bishop, J. R. Abelson, *J. Appl. Phys.* **2014**, 115, 063506.
- [33] T. H. Lee, D. Loke, K. J. Huang, W. J. Wang, S. R. Elliott, *Adv. Mater.* **2014**, 26, 7493.
- [34] P. M. Voyles, D. A. Muller, *Ultramicroscopy* **2002**, 93, 147.
- [35] G. Adam, J. H. Gibbs, *J. Chem. Phys.* **1965**, 43, 139.
- [36] L. M. Martinez, C. A. Angell, *Nature* **2001**, 410, 663.
- [37] Y. Gueguen, J.-C. Sangleboeuf, V. Keryvin, T. Rouxel, E. A. King, E. Robin, G. Delaizir, B. Bureau, X.-H. Zhang, P. Lucas, *J. Ceram. Soc. Jpn.* **2008**, 116, 890.
- [38] M. Salinga, E. Carria, A. Kaldenbach, M. Bornhöft, J. Benke, J. Mayer, M. Wuttig, *Nat. Commun.* **2013**, 4, 2371.
- [39] D. Turnbull, *Contemp. Phys.* **1969**, 10, 473.
- [40] J. Orava, A. L. Greer, *Acta Mater.* **2017**, 139, 226.
- [41] J. Q. Wang, Y. Shen, J. H. Perepezko, M. D. Ediger, *Acta Mater.* **2016**, 104, 25.
- [42] V. Velikov, S. Borick, C. A. Angell, *Science* **2001**, 294, 2335.
- [43] M. Schumacher, H. Weber, P. Jávári, Y. Tsuchiya, T. G. A. Youngs, I. Kaban, R. Mazzarello, *Sci. Rep.* **2016**, 6, 27434.
- [44] J. Mauro, Y. Yue, A. J. Ellison, P. Gupta, D. Allan, *Proc. Natl. Acad. Sci. USA* **2009**, 106, 19780.
- [45] C. T. Moynihan, S. K. Lee, M. Tatsumisago, T. Minami, *Thermochim. Acta* **1996**, 280–281, 153.
- [46] V. Velikov, S. Borick, C. A. Angell, *J. Phys. Chem. B* **2002**, 106, 1069.
- [47] H. S. Chen, E. Coleman, *Appl. Phys. Lett.* **1976**, 28, 245.
- [48] Y. Z. Yue, S. L. Jensen, J. deC. Christiansen, *Appl. Phys. Lett.* **2002**, 81, 2983.
- [49] J. Huang, P. K. Gupta, *J. Non-Cryst. Solids* **1992**, 151, 175.
- [50] L. Hu, Y. Yue, *J. Phys. Chem. B* **2008**, 112, 9053.
- [51] H. J. Borchardt, F. Daniels, *J. Am. Chem. Soc.* **1957**, 79, 41.
- [52] R. L. Blaine, H. E. Kissinger, *Thermochim. Acta* **2012**, 540, 1.
- [53] K. L. Ngai, *Phys. Rev. E* **1998**, 57, 7346.
- [54] H. Weber, J. Orava, I. Kaban, J. Pries, A. L. Greer, *Phys. Rev. Mater.* **2018**, 2, 093405.
- [55] W. Zhang, A. Thiess, P. Zalden, R. Zeller, P. H. Dederichs, J. Y. Raty, M. Wuttig, S. Blugel, R. Mazzarello, *Nat. Mater.* **2012**, 11, 952.
- [56] A. S. Okhotin, A. N. Krestovnikov, A. A. Aivazov, A. S. Pushkarskii, *Phys. Status Solidi B* **1969**, 31, 485.